Research Article | Vol. 27, No. 17 | 19 Aug 2019 | OPTICS EXPRESS 24072
Optics EXPRESS

Selective wavelength conversion in a few-mode fiber

OMAR F. ANJUM,[1,*] MASSIMILIANO GUASONI,[1] PETER HORAK,[1] YONGMIN JUNG,[1] MASATO SUZUKI,[2] TAKEMI HASEGAWA,[2] KYLE BOTTRILL,[1] DAVID J. RICHARDSON,[1] FRANCESCA PARMIGIANI,[1,3] AND PERIKLIS PETROPOULOS[1]

[1] *Optoelectronics Research Centre, University of Southampton, Southampton SO17 1BJ, UK*
[2] *Optical Communications Laboratory, Sumitomo Electric Industries, Ltd., Yokohama 244-8588, Japan*
[3] *Currently at Microsoft Research, Cambridge, CB1 2FB, UK*
[*] *o.f.anjum@soton.ac.uk*

Abstract: We experimentally demonstrate a means to selectively enhance wavelength conversion of WDM channels on a 100 GHz grid exploiting nonlinear effects between the spatial modes of a few mode fiber. The selectivity of parametric gain is obtained by dispersion design of the fiber such that the inverse group velocity curves of the participating modes are parallel and their dispersion is suitably large. We describe both theoretically and experimentally the observed dependence of the idler gain profile on pump mode (quasi) degeneracy.

1. Introduction

Parametric processes arising from the $\chi^{(3)}$ nonlinearity have already been exploited to implement a number of signal processing functionalities. These include, for instance, all-optical amplification of signals, phase-sensitive amplification and wavelength conversion [1–3]. Most demonstrations involving these functionalities have been based on single-mode waveguides, such as highly nonlinear fibers and silicon photonic devices, where it has been shown that efficient generation of parametric effects over broad spectral ranges is possible through sophisticated dispersion engineering. Broadband performance requires operating near the zero dispersion wavelength of the waveguide and maintaining low dispersion across the wavelengths of interest; the challenges in the design and implementation of such optical waveguide properties should not be underestimated. Furthermore, a pitfall of having low dispersion in single-mode nonlinear systems is that it gives rise to unintended interactions between the input waves, such as four-wave mixing (FWM) induced signal-to-signal crosstalk [4]. If the objective is to act on a specific signal wavelength (such as for amplification or wavelength conversion), then accurate control over fourth-order dispersion (β_4) [5] is needed, which is difficult to achieve due to design and fabrication challenges.

While inter-modal (IM) FWM was first demonstrated several decades ago [6], inter-modal nonlinear phenomena in waveguides have been the subject of renewed theoretical and experimental interest due to the rich and complex behaviour they exhibit [7–10] and because of their relevance in emerging communications, fiber laser and quantum technologies [11–19]. For example, some limitations of the single-mode systems mentioned above can be overcome if more than one spatial mode of the waveguide can be allowed to interact nonlinearly. This allows the opportunity for exploiting additional degrees of freedom: not only can frequencies in the same mode interact by mediation of $\chi^{(3)}$, but now each frequency and mode pair can be coupled nonlinearly to another such pair as part of an inter-modal (IM) FWM interaction. This fact, along with the ability to

#368837 https://doi.org/10.1364/OE.27.024073
Journal © 2019 Received 3 Jun 2019; revised 10 Jul 2019; accepted 10 Jul 2019; published 7 Aug 2019

Optics EXPRESS

dispersion engineer the modes of a waveguide, can provide additional control over certain signal processing functionalities. Recently, we used inter-modal (IM) FWM Bragg Scattering [20] (discussed in the following section) for wavelength conversion of optical signals from the C-band to the L-band using a few-mode fiber (FMF) [21], and the same was done in a silicon waveguide in a separate work [22]. Dispersion engineering of the waveguides was also used to further enhance the bandwidths over which the conversion was achieved [23, 24].

More recently, we demonstrated preliminary results on a new application of IM FWM: the selective conversion of wavelength division multiplexed (WDM) channels on a 100 GHz grid [25]. This was achieved by exploiting IM FWM Bragg Scattering between the spatial modes of a few-mode fiber (FMF). In this paper, we expand on that study and investigate experimentally and numerically the influence of pump mode degeneracy on channel selectivity.

2. Selective inter-modal Bragg scattering

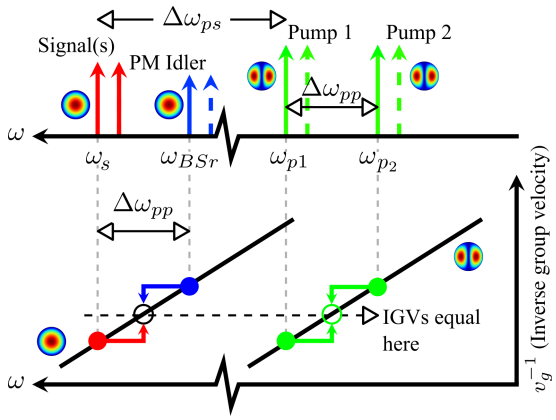

Fig. 1. The wave configuration used in the experiment in which the pumps are in a higher order mode and the signal is in the fundamental mode. The modes and wavelengths are shown at the top, whereas the inverse group velocity curves and their relationship with phase matching are shown at the bottom.

The principle of IM FWM Bragg Scattering is shown in Fig. 1. To illustrate the concept, we assume the fiber to be isotropic with fully degenerate mode groups. The pumps (in mode LP_{11}) are at frequencies ω_{p1} and ω_{p2}, while the first of the two signals (in mode LP_{01}) lies at ω_s. As seen in the top part of Fig. 1, a Bragg Scattering idler, whose frequency is determined by energy conservation, emerges at $\omega_{BSr} = \omega_s + \omega_{p2} - \omega_{p1}$ (see the wave marked as PM Idler in the figure).

The spatial mode diversity of this scheme has a significant role in phase-matching the process. The (relative) inverse group velocity (IGV) curves of the two participating modes are shown at the bottom of Fig. 1. Phase matching is achieved for the PM Idler if v_g^{-1} evaluated at the average of the frequencies in mode LP_{11} (i.e. the pump frequencies) equals v_g^{-1} evaluated at the average of the two frequencies belonging to mode LP_{01} [19, 23]. This is depicted by the horizontal dashed line in Fig. 1. Therefore, maximum idler generation at ω_{BSr} occurs when the signal is placed at a separation $\Delta\omega_{ps}$ from the pumps. Any other signals present in the vicinity, such as the second signal shown in red in the Fig. 1, are expected not to undergo efficient conversion. Further, phase-matching can only hold when the pumps located at ω_{p1} and ω_{p2} are in the LP_{11} mode, since the IGV curves of other higher-order modes will not generally satisfy the condition presented in Fig. 1. The higher the dispersion (or IGV slopes), the faster the 'average' IGVs get displaced from each other, and the narrower the bandwidth of signal frequencies over which idler gain is available.

Optics EXPRESS

If the IGV curves are *parallel*, then we can select the signal to be converted by shifting the pump frequencies accordingly. For example, in order to convert the second signal (shown to the right of ω_s) in Fig. 1, the pump frequencies need to be shifted to those given by the dashed green lines. This will result in the idler generation at the dashed blue line being phase-matched (values of v_g^{-1} at the new average frequencies will match), whereas the first idler should now be far from phase-matching (provided that the dispersion is high enough).

It is worth noting that this scheme does not require the zero dispersion wavelength to take a specific value, as is needed for phase-matching in single-mode systems. Waveguide designs incorporating high dispersion can therefore be used to suppress FWM induced signal-to-signal crosstalk. In addition, in this specific configuration, the signal-idler pair can be far from the pump wavelengths, and hence away from any noise associated with amplified spontaneous emission (ASE) from high power amplifiers or stimulated Raman scattering.

Based on previous work on the same FMF [23], the optimal wavelength separation (in the C-band), for the kind of phase-matching described above, corresponds to $\Delta\lambda_{ps} \approx 22.8$ nm. The dispersion (which is also the slope of the IGV curves in Fig. 2) for mode LP_{01} (LP_{11}) was estimated to be 12.5 ps/nm/km (11.4 ps/nm/km).

3. Experimental details

Our experiments were carried out on a 25.3 μm core-diameter, 100 m long graded index (GI) FMF [23] with a highly GeO_2-doped SiO_2 core. The FMF had a parabolic index profile with a fitted alpha-power of 2.1. While the total number of supported modes in the C-band exceeded ten, the fiber was fabricated in order to achieve phase-matching in a Bragg Scattering process involving the LP_{01} and LP_{11} modes [23]. Effective areas for the modes were calculated to be 55.7 μm^2 (LP_{01}) and 75.6 μm^2 (LP_{11}). A propagation loss of around 0.3 dB/km was measured for the LP_{01} mode.

The experimental set-up for investigating IM FWM is shown in Fig. 2. Also shown are the experimentally measured relative inverse group velocity (RIGV) curves of the modes of interest for our FMF. These measurements have previously been discussed in [23], and their significance [19, 21] in the context of the current work will be further elaborated in the next section. The inputs consisted of two L-band continuous-wave (CW) pumps and a C-band signal. The pumps underwent amplification and their combined power was estimated at 23.5 dBm at the input of the FMF. Pump light successively went through a polarization controller, a polarizing beam splitter (PBS) and a rotating $\lambda/2$ plate in order to obtain linearly polarized light whose angle could be varied. A phase-plate was used to launch the free-space pump beam into the LP_{11} mode of the GI FMF. The signal was combined with the pumps via a beam-splitter (BS) cube and was coupled to the LP_{01} mode of the fiber. To increase the modal purity of the pumps, a two-mode fiber (TMF) ($\sim$ 1 m) was spliced to the input of the GI FMF. This made it easier to match the spatial profile of the LP_{11} mode in the GI FMF, and achieve enhanced selective excitation into this mode. Any LP_{01} mode output was directed through free-space into a single-mode fiber (SMF) and then into an optical spectrum analyzer (OSA), with the LP_{11} mode pumps being rejected automatically due to coupling and propagation losses of higher-order-mode light in an SMF. A modal purity of approximately 20 dB was achieved.

4. Idler gain profile and pump polarization

We now present the results of some basic experimental studies of the ideas presented in the preceding section. Using a single signal in the Bragg scattering system of Fig. 1, we investigated the efficiency of idler generation around the optimum signal wavelength (determined by the pump-signal spacing $\Delta\lambda_{ps}$). We set $\lambda_{p1} = 1570$ nm and $\lambda_{p2} = 1574$ nm (i.e. $\Delta\lambda_{pp} = 4$ nm), and varied the (CW) signal wavelength around the phase-matched location. The input signal power was approximately 8.5 dBm. The pumps were linearly co-polarized at the input, and their angle of

Optics EXPRESS

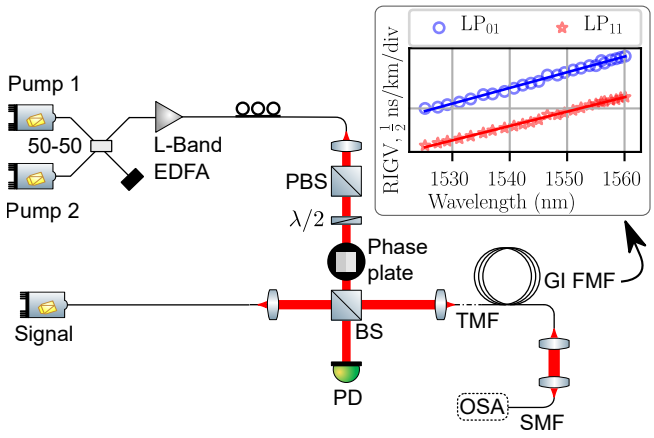

Fig. 2. Experimental setup of the wavelength converter. Also shown are the relative inverse group velocity (or relative β_1) curves of modes LP_{01} and LP_{11} of the few-mode fiber.

polarization (with respect to a fixed direction orthogonal to the path of the beam) could be varied through the combination of a polarizer and $\lambda/2$ waveplate. The state of polarization at the signal was not controlled or varied. We recorded the idler power as a function of signal wavelength for a number of different pump polarization angles, and a selection of such measurements for polarization angle increments of 45° is shown in Figs. 3(a)-(c).

The results indicate that the optimal pump-signal separation $\Delta\omega_{ps}$ is not strictly defined, and the idler gain does not always exhibit a global maximum at a single value of $\Delta\omega_{ps}$ (compare, for instance, Figs. 3(b) and 3(c)).

Further, it was seen that by changing the pump state of polarization arbitrarily (i.e. by removing the PBS and adjusting the polarization controller so the state was no longer linear), it was possible to obtain gain profiles exhibiting narrower peaks. One such example is shown in Fig. 4 ($\Delta\lambda_{pp}$ = 5 nm here). The local minima adjacent to the main peak at 1547 nm are each located about 100 GHz away from it, and the 3-dB bandwidth of the central peak is 0.74 nm (approximately 90 GHz). These results were stable over long periods of time and repeatable, provided that the fiber was not deliberately perturbed.

In order to explain the variation of idler gain observed above, we begin by noting that optical fibers are subject to manufacturing imperfections, environmental variations and local mechanical stress that induce random perturbations in the fiber structure [26]. This breaks the degeneracy of modes in the same group, which separate into a distinct set of quasi-degenerate modes. Differently from degenerate modes, all of which possess the same effective index n, quasi-degenerate modes are characterized by distinct indices that are slightly different. In the following, we indicate the difference $n_j - n_k$ between the effective indexes n_j and n_k of the LP modes j and k with $\Delta n_{j,k}$.

The fundamental mode has been widely studied in the literature, and it is well known that $\Delta n_{01x,01y}$ between the two polarisation modes in a standard single-mode fibre is of the order of 10^{-8} - 10^{-7} [27]. However, we are unaware of any direct measurements of the index difference among polarization modes of the LP_{11} group. We have therefore performed systematic finite-element-method simulations to compute the modes of group LP_{11} and their effective index in the presence of weak perturbations of the fiber structure, such as might result from a slight ellipticity of the transverse section. These simulations reveal that $\Delta n_{11ax,11ay}$ and $\Delta n_{11bx,11by}$ are also of the order of 10^{-8} - 10^{-7}. However, the index difference between one mode of subgroup LP_{11a} and one mode of subgroup LP_{11b}, as for example $\Delta n_{11ax,11bx}$ or $\Delta n_{11ax,11by}$, is typically two orders of magnitude larger.

We ascribe this substantial difference to the different spatial distribution of modes in subgroups

Optics EXPRESS

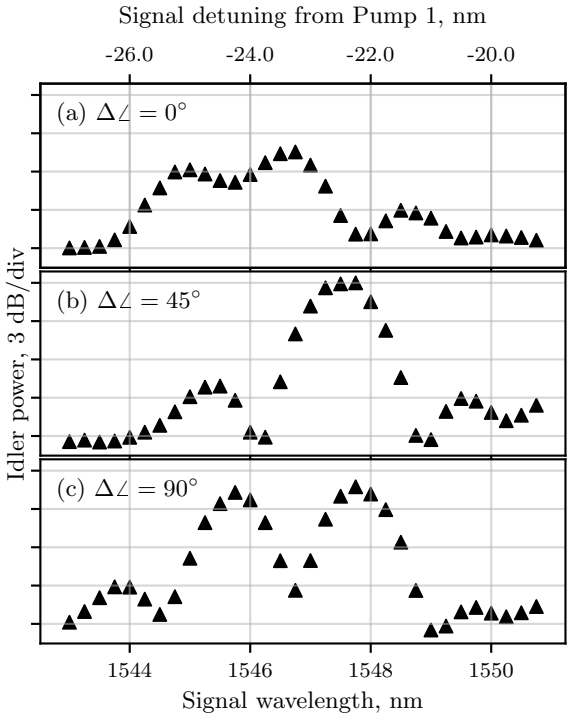

Fig. 3. Measured dependence of gain profile on input polarization angle.

LP_{11a} and LP_{11b}. Consider for example LP_{11ax} and LP_{11bx}. Whenever the perturbation is localized in the proximity of the lobes of one mode, that mode undergoes a much larger variation of the refractive index with respect to the other mode, which in turn results in a large index difference $\Delta n_{11ax,11bx}$. On the contrary, polarization modes of the same subgroup, like LP_{11ax} and LP_{11ay}, possess the same spatial distribution and therefore, in the presence of perturbations, they undergo almost the same variation of their effective index, which in turn results in an extremely small difference $\Delta n_{11ax,11ay}$. In addition, it turns out that the effective index difference between modes of subgroups LP_{11a} and LP_{11b} is almost unaffected by polarization, that is to say, $\Delta n_{11ax,11bx} \approx \Delta n_{11ax,11by} \approx \Delta n_{11ay,11bx} \approx \Delta n_{11ay,11by}$, and in the following this is therefore indicated as Δn_{11ab}.

Due to the aforementioned large effective index difference, subgroups LP_{11a} and LP_{11b} propagate with a different group velocity in the fiber. This difference is quantified through the differential inverse group velocity $\mathrm{dIGV}_{11ab} = \Delta n_{11ab}/c$. In practice, this means that two distinct FWM processes are possible, each involving mode LP_{01} and one of the LP_{11a} and LP_{11b} modes. As illustrated in Fig. 5, for fixed pump wavelengths these processes are phase-matched at different signal wavelengths.

When the input pumps are coupled to the LP_{11a} modes, only the first FWM process occurs: phase-matching (and maximum idler generation) is achieved at a signal wavelength λ_a (or frequency ω_a). When the input pump is coupled to LP_{11b} modes, only the second FWM process occurs and maximum idler conversion is achieved at a different signal wavelength λ_b. The difference $\lambda_b - \lambda_a = \mathrm{dIGV}_{11ab}/D$ (where D is the dispersion parameter, or equivalently $\omega_b - \omega_a = \mathrm{dIGV}_{11ab}/\beta_2$) defines the range of tunability of the peak gain. In the realistic case where $\Delta n_{11ab} \sim 10^{-5}$, it is of the order of a few nanometers.

Optics EXPRESS

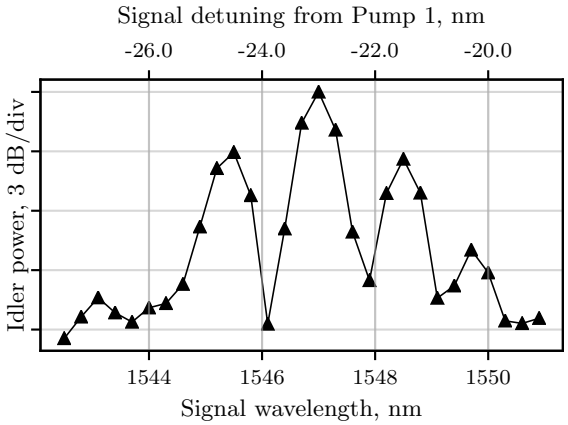

Fig. 4. Measured variation of (normalized) idler power with signal wavelength in the case when pump polarization is chosen to give narrow bandwidth peaks.

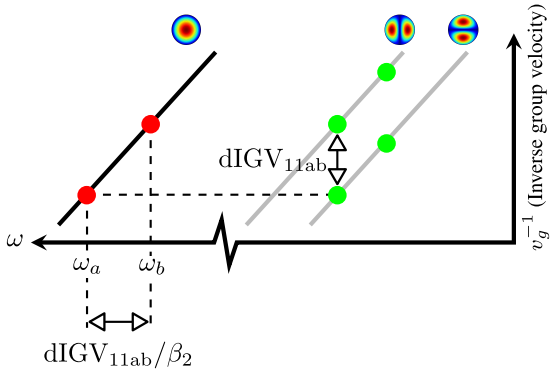

Fig. 5. Having slightly different dispersion characteristics for the spatial modes within the group LP_{11} changes the optimal signal frequency.

Figure 6 displays the related gain profiles as obtained from numerical simulations. In these simulations we use fiber parameters and birefringence axes that move randomly along the fiber length as a result of random perturbations [28]. Figure 6(a) shows the calculated gain curves which are obtained when all the pump energy is contained in either the LP_{11a} or LP_{11b} mode. Idler gain is maximized at distinctly different wavelengths in the two cases. But when the input pumps are simultaneously coupled to subgroups LP_{11a} and LP_{11b}, then both are involved in the IM FWM process. In this case, the gain curve depends on the specific amount of power coupled into the two subgroups, and can take a form that is a composite of the two curves presented in Fig. 6(a). Some examples of this are presented in Fig. 6(b). In broad terms, the composite gain is a combination of the LP_{11a}- and LP_{11b}-only gain curves and may exhibit multiple peaks whose wavelengths may not coincide with those observed in Fig. 6(a).

These observations are in good agreement with the results in Fig. 3: by varying the polarization angle of the pump beam at the fiber input, we effectively change the amount of pump power coupled to subgroups LP_{11a} and LP_{11b} into the fibre [29]). Specifically, the LP_{11} pump at ω_{p1} experiences a change in the distribution of power between subgroups LP_{11a} and LP_{11b} (ditto for the pump at ω_{p2}). This linear exchange of power between the pump subgroups was also

Optics EXPRESS

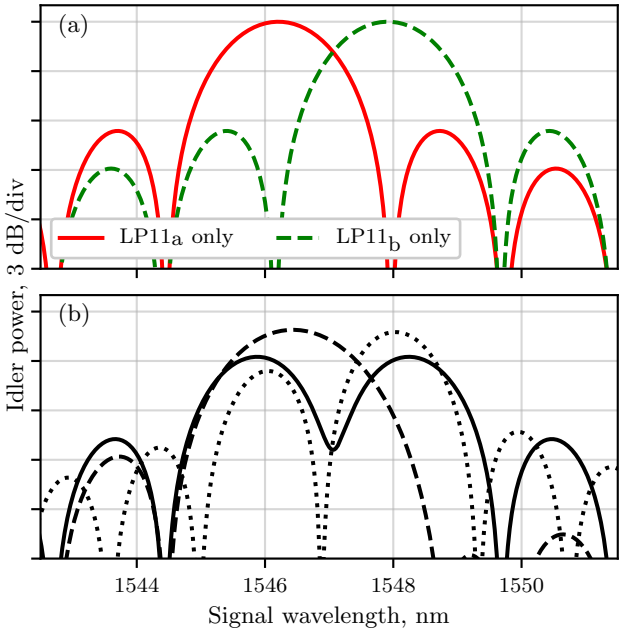

Fig. 6. (a) Simulated gain profiles in which pump energy is contained exclusively in either LP_{11a} or LP_{11b}. (b) Simulated gain profiles in which pump energy is coupled to both subgroups.

verified experimentally by setting up a mode demultiplexer. The demultiplexer was based on phase-plates of the same type used to launch the higher-order LP_{11} mode (as shown in Fig. 2). These phase-plates are holographic optical elements that, in addition to selective mode excitation, can be used for the modal decomposition of the output beam into its spatial subgroups (see eg. [30, 31]). Then, following the reasoning given in the preceding paragraphs, this results in a change in the shape of the gain profile. Multiple peaks can be generated and the range of tunability of the gain peak in Fig. 3 is about 3 nm (1545-1548 nm), which confirms our previous estimate.

Based on the above discussion, we should expect that if the input configuration is changed to one in which the pumps are in the fundamental (LP_{01}) mode group and the signal is in LP_{11}, there should be minimal impact of pump polarization on idler gain. This is because when we vary the polarization of the pump beams so as to change the amount of pump power coupled to the LP_{01x} and LP_{01y} modes, the differential group velocity among them (LP_{01x} and LP_{01y}) is extremely small when compared to the previous case, which results in a range of tunability of peak gain as small as 0.01 nm. Since this range is much smaller than the gain bandwidth, in practice we should not observe any difference in the gain profile, regardless of the input polarization of the pumps.

This was tested by switching the pumps to LP_{01} and letting $\lambda_{p1} = 1550$ nm and $\lambda_{p2} = 1554$ nm, while varying the LP_{11} signal around the optimum offset ($\Delta\lambda_{ps} \approx 22.8$ nm). A mode demultiplexer [31] was set up to accept the LP_{11} fields. The idler gain profile is shown in Fig. 7. As expected, in this modified configuration, it was observed that changing the pump polarization has a minor impact on the overall shape of the profile (compare with Fig. 3).

Optics EXPRESS

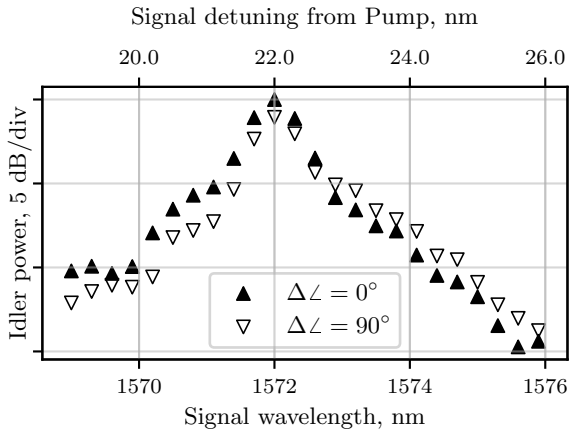

Fig. 7. Change in idler power profile when the mode configuration is switched to having the pumps in the fundamental mode and the signal in the higher order mode.

5. Selective channel conversion

We next set up a WDM experiment to demonstrate channel selectivity in wavelength conversion based on the principles presented above. The mode configuration shown in Fig. 1 was employed, now with three signal inputs with equal powers. Three 10 GHz OOK signal channels centered at 193.3 THz (≈ 1550.9 nm) and separated by 100 GHz (≈ 0.8 nm) were amplified and launched into the LP_{01} mode with a total power of 18 dBm into the fiber (stable idler demodulation was demonstrated previously in [25]). After signal amplification, any amplified spontaneous emission (ASE) from the erbium-doped fiber amplifier (EDFA) outside the band of the signals was filtered away to preserve the optical signal to noise ratio (OSNR) of the generated IM FWM idlers. The polarization of the input signals was kept linear and co-polarized to one another.

The spectra in Figs. 8(a)-(c) show experimental results obtained as the two pumps were tuned in increments of 100 GHz. The signals are denoted by λ_i ($i = 1, 2, 3$) and the corresponding IM FWM idlers are labelled λ_i'. The pumps are labelled as P1 and P2, and $\Delta\lambda_{ps}$ was kept equal to 22.8 nm at all times, i.e. the wavelength separation between the signal of interest and the pumps was kept at this fixed value. To keep the idlers well separated in wavelength from the signals, $\Delta\lambda_{pp}$ was maintained at 5.15 nm. The sharp drop in power around the spectral region of the signals is due to the filtering mentioned above. Also visible are idler peaks resulting from intra-modal FWM among the signals in LP_{01}, at either side of the signal wavelengths.

Once the pump wavelengths had been tuned appropriately for conversion of a given channel, a polarization controller was used to adjust pump polarization (not necessarily linear) to further optimize idler selectivity. Fig. 8(a) shows Pump 1 (P1) and signal λ_1 separated by about 22.8 nm from each other. Clearly, out of the three signals, λ_1 is converted most efficiently to the idler denoted by λ_1', with an extinction ratio of about 16 dB relative to the other idlers. Next, by tuning the pumps to achieve a separation of 22.8 nm with signal λ_2, and subsequently adjusting (pump) polarization to optimize idler generation at λ_2' results in the situation in Fig. 8(b). Similarly, Fig. 8(c) shows the case for the selective generation of idler λ_3'. In all cases, extinction ratios in excess of 10.0 dB were achieved.

Optics EXPRESS

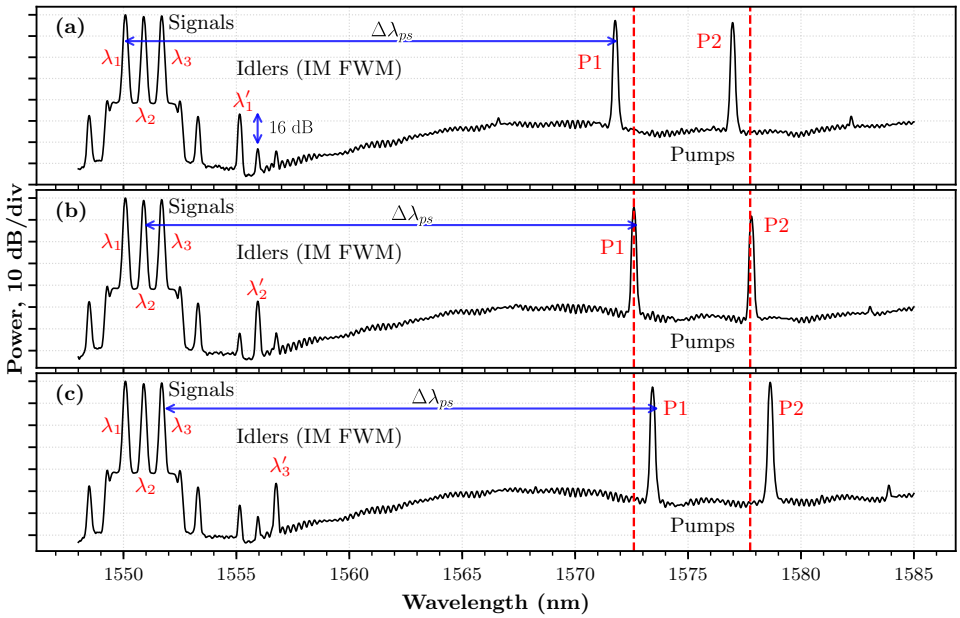

Fig. 8. (a)-(c) Spectra at the LP_{01} port when the pumps are scanned in increments of 100 GHz for conversion to idlers λ_1', λ_2' and λ_3' respectively.

6. Conclusions

We have exploited IM FWM in a dispersive FMF to achieve selective wavelength conversion of individual WDM channels on a 100 GHz spacing. Our configuration employed pumps in the LP_{11} mode and kept the signal in the fundamental mode. We have also discussed the role of mode group degeneracy in further controlling the selectivity. It was found that pump wavelength could be used in conjunction with (pump) polarization, which effectively controlled coupling to the individual spatial modes within the LP_{11} mode group, to tune the idler gain profile. We were able to achieve up to 16 dB power extinction between the channel of interest and the other wavelength channels.

Funding

Engineering and Physical Sciences Research Council (EP/P026575/1, EP/S002871/1).

References

1. M. Marhic, *Fiber Optical Parametric Amplifiers, Oscillators and Related Devices* (Cambridge University, 2007).
2. K. K. Chow, C. Shu, and A. Bjarklev, "Polarization-insensitive widely tunable wavelength converter based on four-wave mixing in a dispersion-flattened nonlinear photonic crystal fiber," IEEE Photonics Technol. Lett. **17**, 624–626 (2005).
3. M. A. Foster, A. C. Turner, J. E. Sharping, B. S. Schmidt, M. Lipson, and A. L. Gaeta, "Broad-band optical parametric gain on a silicon photonic chip," Nature **441**, 960 EP – (2006).
4. M. E. Marhic, P. A. Andrekson, P. Petropoulos, S. Radic, C. Peucheret, and M. Jazayerifar, "Fiber optical parametric amplifiers in optical communication systems," Laser & Photonics Rev. **9**, 50–74 (2015).
5. M. Hirano, T. Nakanishi, T. Okuno, and M. Onishi, "Selective fwm-based wavelength conversion realized by highly nonlinear fiber," in *2006 European Conference on Optical Communications,* vol. 4 (2006), pp. 21–22.
6. R. H. Stolen, J. E. Bjorkholm, and A. Ashkin, "Phase-matched three-wave mixing in silica fiber optical waveguides," Appl. Phys. Lett. **24**, 308–310 (1974).

Optics EXPRESS

7. L. G. Wright, W. H. Renninger, D. N. Christodoulides, and F. W. Wise, "Spatiotemporal dynamics of multimode optical solitons," Opt. Express **23**, 3492–3506 (2015).
8. L. G. Wright, Z. Liu, D. A. Nolan, M.-J. Li, D. N. Christodoulides, and F. W. Wise, "Self-organized instability in graded-index multimode fibres," Nat Photon **10**, 771–776 (2016). Article.
9. M. E. V. Pedersen, J. Cheng, C. Xu, and K. Rottwitt, "Transverse field dispersion in the generalized nonlinear schrödinger equation: Four wave mixing in a higher order mode fiber," J. Light. Technol. **31**, 3425–3431 (2013).
10. M. Ziemienczuk, A. M. Walser, A. Abdolvand, and P. S. J. Russell, "Intermodal stimulated raman scattering in hydrogen-filled hollow-core photonic crystal fiber," J. Opt. Soc. Am. B **29**, 1563–1568 (2012).
11. D. J. Richardson, J. M. Fini, and L. E. Nelson, "Space-division multiplexing in optical fibres," Nat Photon **7**, 354–362 (2013). Review.
12. S. Mumtaz, R.-J. Essiambre, and G. P. Agrawal, "Nonlinear propagation in multimode and multicore fibers: Generalization of the manakov equations," J. Light. Technol. **31**, 398–406 (2013).
13. G. Rademacher, R. S. LuÃŋs, B. J. Puttnam, H. Furukawa, R. Maruyama, K. Aikawa, Y. Awaji, and N. Wada, "Investigation of intermodal four-wave mixing for nonlinear signal processing in few-mode fibers," IEEE Photonics Technol. Lett. **30**, 1527–1530 (2018).
14. G. Rademacher, R. S. LuÃŋs, B. J. Puttnam, Y. Awaji, M. Suzuki, T. Hasegawa, and N. Wada, "Wide-band intermodal wavelength conversion in a dispersion engineered highly nonlinear fmf," in *2019 Optical Fiber Communications Conference and Exhibition (OFC),* (2019), W1C.4.
15. L. G. Wright, D. N. Christodoulides, and F. W. Wise, "Spatiotemporal mode-locking in multimode fiber lasers," Science **358**, 94–97 (2017).
16. S. Signorini, S. Piccione, M. Ghulinyan, G. Pucker, and L. Pavesi, "Are on-chip heralded single photon sources possible by intermodal four wave mixing in silicon waveguides?" in *SPIE Proceedings Volume 10733, Quantum Photonic Devices,* vol. 10733 (2018).
17. K. Garay-Palmett, D. Cruz-Delgado, F. Dominguez-Serna, E. Ortiz-Ricardo, J. Monroy-Ruz, H. Cruz-Ramirez, R. Ramirez-Alarcon, and A. B. U'Ren, "Photon-pair generation by intermodal spontaneous four-wave mixing in birefringent, weakly guiding optical fibers," Phys. Rev. A **93**, 033810 (2016).
18. R. J. Essiambre, M. A. Mestre, R. Ryf, A. H. Gnauck, R. W. Tkach, A. R. Chraplyvy, Y. Sun, X. Jiang, and R. Lingle, "Experimental investigation of inter-modal four-wave mixing in few-mode fibers," IEEE Photonics Technol. Lett. **25**, 539–542 (2013).
19. S. M. M. Friis, I. Begleris, Y. Jung, K. Rottwitt, P. Petropoulos, D. J. Richardson, P. Horak, and F. Parmigiani, "Inter-modal four-wave mixing study in a two-mode fiber," Opt. Express **24**, 30338–30349 (2016).
20. C. J. McKinstrie and S. Radic, "Parametric amplifiers driven by two pump waves with dissimilar frequencies," Opt. Lett. **27**, 1138–1140 (2002).
21. F. Parmigiani, P. Horak, Y. Jung, L. Grüner-Nielsen, T. Geisler, P. Petropoulos, and D. J. Richardson, "All-optical mode and wavelength converter based on parametric processes in a three-mode fiber," Opt. Express **25**, 33602–33609 (2017).
22. C. Lacava, M. A. Ettabib, T. D. Bucio, G. Sharp, A. Z. Khokhar, Y. Jung, M. Sorel, F. Gardes, D. J. Richardson, P. Petropoulos, and F. Parmigiani, "Intermodal bragg-scattering four wave mixing in silicon waveguides," J. Light. Technol. **37**, 1680–1685 (2019).
23. O. F. Anjum, P. Horak, Y. Jung, M. Suzuki, Y. Yamamoto, T. Hasegawa, P. Petropoulos, D. J. Richardson, and F. Parmigiani, "Bandwidth enhancement of inter-modal four wave mixing bragg scattering by means of dispersion engineering," APL Photonics **4**, 022902 (2019).
24. C. Lacava, T. D. Bucio, A. Z. Khokhar, P. Horak, Y. Jung, F. Y. Gardes, D. J. Richardson, P. Petropoulos, and F. Parmigiani, "Intermodal frequency generation in silicon-rich silicon nitride waveguides," Photon. Res. **7**, 615–621 (2019).
25. O. F. Anjum, K. Bottrill, P. Horak, Y. Jung, M. Suzuki, Y. Yamamoto, T. Hasegawa, D. J. Richardson, F. Parmigiani, and P. Petropoulos, "Channel selective wavelength conversion by means of inter modal four wave mixing," in *Optical Fiber Communication Conference (OFC) 2019,* (Optical Society of America, 2019), p. W4F.4.
26. L. Palmieri and A. Galtarossa, "Coupling effects among degenerate modes in multimode optical fibers," IEEE Photonics J. **6**, 1–8 (2014).
27. J. N. Damask, *Polarization optics in telecommunications*, vol. 101 (Springer Science & Business Media, 2004).
28. M. Guasoni, F. Parmigiani, P. Horak, J. Fatome, and D. J. Richardson, "Intermodal four-wave-mixing and parametric amplification in km-long multi-mode fibers," J. Light. Technol. **35**, 5296 – 5305 (2017).
29. S. Randel, R. Ryf, A. Sierra, P. J. Winzer, A. H. Gnauck, C. A. Bolle, R.-J. Essiambre, D. W. Peckham, A. McCurdy, and R. Lingle, "6×56-gb/s mode-division multiplexed transmission over 33-km few-mode fiber enabled by 6×6 mimo equalization," Opt. Express **19**, 16697–16707 (2011).
30. R. Ryf, C. Bolle, and J. von Hoyningen-Huene, "Optical coupling components for spatial multiplexing in multi-mode fibers," in *37th European Conference and Exposition on Optical Communications,* (Optical Society of America, 2011), p. Th.12.B.1.
31. O. F. Anjum, M. Guasoni, P. Horak, Y. Jung, P. Petropoulos, D. J. Richardson, and F. Parmigiani, "Polarization insensitive four wave mixing based wavelength conversion in few-mode optical fibers," J. Light. Technol. pp. 3678 – 3683 (2018).